ACS APPLIED MATERIALS & INTERFACES

Research Article

www.acsami.org

Demonstration of Ultrarapid Interfacial Formation of 1D Fullerene Nanorods with Photovoltaic Properties

Rekha Goswami Shrestha,[†,‡] Lok Kumar Shrestha,[*,‡] Ali Hossain Khan,[§] Gundam Sandeep Kumar,[§] Somobrata Acharya,[*,§] and Katsuhiko Ariga[‡,∥]

[†]Catalytic Materials Group, Environmental Remediation Materials Unit, Environment and Energy Materials Division, National Institute for Materials Science (NIMS) , 1-1 Namiki, Tsukuba, Ibaraki 305-0044 Japan

[‡]International Center for Materials Nanoarchitectonics (WPI-MANA), National Institute for Materials Science (NIMS), 1-1 Namiki, Tsukuba Ibaraki 305-0044, Japan

[§]Centre for Advanced Materials (CAM), Indian Association for the Cultivation of Science, Jadavpur, Kolkota 700 032, India

[∥]Core Research for Evolutional Science and Technology (CREST), Japan Science and Technology Agency (JST), 1-1 Namiki, Tsukuba Ibaraki 305-0044, Japan

Supporting Information

ABSTRACT: We demonstrate ultrarapid interfacial formation of one-dimensional (1D) single-crystalline fullerene C_{60} nanorods at room temperature in 5 s. The nanorods of ~11 μm in length and ~215 nm in diameter are developed in a hexagonal close-pack crystal structure, contrary to the cubic crystal structure of pristine C_{60}. Vibrational and electronic spectroscopy provide strong evidence that the nanorods are a van der Waals solid, as evidenced from the preservation of the electronic structure of the C_{60} molecules within the rods. Steady state optical spectroscopy reveals a dominance of charge transfer excitonic transitions in the nanorods. A significant enhancement of photogenerated charge carriers is observed in the nanorods in comparison to pristine C_{60}, revealing the effect of shape on the photovoltaic properties. Due to their ultrarapid, large-scale, room-temperature synthesis with single-crystalline structure and excellent optoelectronic properties, the nanorods are expected to be promising for photosensitive devices applications.

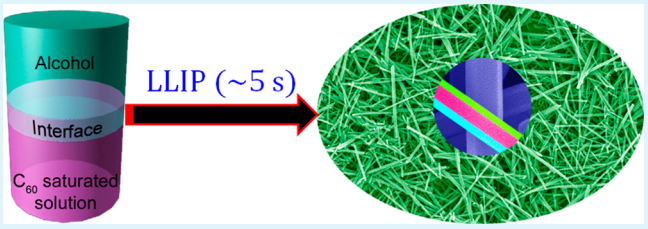

KEYWORDS: *fullerene single-crystal nanorods, ultrarapid crystal formation, liquid−liquid interfacial precipitation, photoluminescence, photovoltaic properties*

1. INTRODUCTION

One-dimensional (1D) single-crystal nanorods or nanotubes consisting of functional fullerene C_{60} possess unique physical and chemical properties due to the presence of novel conjugated π-systems.[1−4] These 1D nanostructures derived from ideally zero-dimensional (0D) molecules possess unique optoelectronic properties including high electron mobility, high photosensitivity, and excellent electron accepting properties. Owing to these attractive features, 1D nanostructures of fullerene C_{60} have received significant interest recently for possible applications in a variety of flexible optoelectronic devices including field effect transistors, light emitting diodes, photovoltaic cells, sensors, and photodetectors.[5−9]

In organic photovoltaics, major attention is focused to develop newer types of donor materials. Fullerene C_{60} has become the most popular electron acceptor material in organic solar cells due to its superior electron conductivity and efficient charge separation capabilities at electron donor/acceptor interfaces.[10−15] Nevertheless, fullerene remains as the main acceptor material, as it matches well with a wide variety of donor materials. For example, semiconducting quantum dots can be used to prepare C_{60} composites for improved capture of photogenerated electrons in quantum dots. Brown and Kamat[16] observed that the photocurrent generation efficiency of CdSe−C_{60} composite film is 2 orders of magnitude higher than pristine CdSe film. Electrical conductivity measurements on a single fullerene nanotube have revealed that the C_{60} tube results in a large photoconductivity under light irradiation that could be promising for optical switching.[17,18] A recent report demonstrated that the photosensitivity of C_{60} nanorods can be enhanced by 400-fold via an ultralow photodoping mechanism.[19] Hence, easy and large-scale room-temperature fabrication of dimension-controlled fullerene C_{60} nanostructures is potentially important for the fabrication of a variety of photosensitive devices.

Fullerene crystal synthesis is a developed field now, and several methods have been reported for the production of shape-controlled C_{60} crystals. Templating, slow evaporation,

Received: July 15, 2014
Accepted: August 18, 2014
Published: August 19, 2014

 © 2014 American Chemical Society

and vapor deposition are some common methods employed to control C_{60} crystals morphology.[20−27] The liquid−liquid interfacial precipitation (LLIP) method developed by Miyazawa and co-workers[28,29] is one of the versatile methods for the fabrication of 1D to higher dimensional crystals of C_{60}, including three-dimensional nanoporous fullerenes.[30−35] However, it generally takes a few days to a week to grow C_{60} crystals using LLIP method. A rapid and large-scale room-temperature synthesis of high-quality fullerene nanostructure is still lacking.

Here, we demonstrate ultrarapid production of fullerene C_{60} nanorods (FNRs) by adding methanol into a saturated solution of C_{60} in mesitylene at room temperature (25 °C). The synthesis is completed in just 5 s, suggesting a major accomplishment over the previously reported methods in terms of reaction time. FNRs are found to be ∼11 μm in length and ∼215 nm in diameter showing hexagonal close-pack crystal structure. Synthesized FNRs were characterized using scanning electron microscopy (SEM), transmission electron microscopy (TEM), powder X-ray diffraction (XRD), Fourier transformed-infrared (FTIR) spectroscopy, Raman scattering, X-ray photoelectron spectroscopy (XPS), UV−vis spectroscopy, and photoluminescence (PL) spectroscopy. Thereafter, we have fabricated photovoltaic cells consisting of FNRs as active layers, which were sandwiched between transparent anode indium tin oxide (ITO) and metal cathode aluminum (Al). A comparison of FNRs with pristine C_{60} reveals an enhanced photovoltaic response for the FNRs, suggesting charge transport under light irradiation.

2. EXPERIMENTAL SECTION

2.1. Materials. Pristine fullerene C_{60} powder with purity >99.5% was purchased from Materials Technologies Research, Ltd. (Cleveland, OH). Methanol and mesitylene with purity >99% were purchased from the Wako Chemical Corporation, Japan. They were used as received.

2.2. Crystal Synthesis. FNRs were prepared using the LLIP method at an interface of methanol and saturated solution of C_{60} in mesitylene at room temperature. A saturated solution of C_{60} in mesitylene (0.99 mg/mL) was prepared by dissolving an excess amount of pristine C_{60} powder in 25 mL mesitylene. Undissolved C_{60} powder was removed by filtration. In a typical crystallization, 1 mL of the saturated solution of C_{60} in mesitylene was placed in a clean and dry glass vial (10 mL) and kept at 25 °C in a temperature-controlled water bath for 30 min. In a different glass vial, 5 mL of methanol was also equilibrated at 25 °C for 30 min. Note that C_{60} is poorly soluble in methanol (0.0004 mg/mL at 25 °C). The 5 mL methanol solution was then added on top of the saturated solution of C_{60} in mesitylene. A brownish color developed instantly, indicating the formation of FNRs.

2.3. Characterizations. The prepared FNRs were subjected to various advanced characterization techniques, including SEM (S-4800, Hitachi Co. Ltd., Japan, operated at 10 kV) and TEM (JEOL Model JEM-2100F, operating at 200 kV). X-ray diffraction patterns were obtained using a Rigaku (Japan) Model RINT2000 diffractometer with Cu Kα radiation (λ = 0.1541 nm) operated at 40 kV and 40 mA. Raman scattering (Raman spectrometer Jobin-Yvon T64000) samples were excited using green laser (514.5 nm, 0.025 mW power). Additionally, the FNRs were characterized using XPS performed on a Sigma Probe spectrometer (Thermo Scientific Co., Ltd., Yokohama, Japan) using monochromated Al Kα radiation (photon energy 1487 eV). For high-resolution spectra, the core level C 1s and O 1s, with sufficient number of scan to ensure a high signal-to-noise ratio, were recorded in 0.05 eV steps. An electron flood gun was used to prevent sample charging. After the linear baseline subtraction, curve fittings were performed assuming a Gaussian peak shape.

2.4. Absorption and Photoluminescence (PL) Spectroscopy. UV/vis absorption spectrum of the FNRs and pristine C_{60} were recorded on a UV/vis spectrometer V-570 at 25 °C in the wavelength range of 200−900 nm. PL spectra of ultrarapidly grown FNRs and pristine C_{60} powder were measured at room temperature in air using a spectrometer equipped with a liquid-nitrogen-cooled CCD detector. Samples were cast on a silicon substrate and excited using the 514.5 nm line of an Ar^+ laser. All the PL spectra are corrected for the wavelength-dependent sensitivity of the photodetection system.

2.5. Photovoltaic Study. We have fabricated photovoltaic cells consisting of thin films of P3HT and FNRs as active layers, which were sandwiched between transparent anode ITO and metal cathode Al using pristine C_{60} and FNRs separately. P3HT was used as the *p*-type donor polymer and C_{60} was used as the *n*-type acceptor in the active layer. The device structure was ITO−poly(3,4-Ethylenedioxythiopene) (PEDOT)/poly(styrenesulfonate) (PSS)−P3HT−C_{60}−Al. At first, ITO-coated glass substrates (Aldrich, 15−25 Ω/sq) were cleaned with detergent, ultrasonicated in acetone and isopropyl alcohol, and subsequently dried overnight in an oven under reduced pressure. Spin-coating was carried out in a fume hood with good ventilation. Chemical preparation, spin-coating, and post annealing were all performed in air. The spin-coater was set at 5000 rpm for 60 s and maximized acceleration and deceleration speeds for PEDOT/PSS (Aldrich) film preparation to modify the ITO surface. Baking of this thin PEDOT/PSS film was carried out in air at 120 °C for 1 h. Then, 15 mg/mL P3HT solution was prepared in 1,2-dichlorobenzene and spin-coated onto the substrates at 2500 rpm for 60 s. The FNRs was drop-casted from its dilute methanol solution. Finally, the cathode (Al, ∼100 nm) was deposited by thermal evaporation under a vacuum of about 10^{-6} Torr. The active area of the device, defined by shadow mask, is 1.5 × 1.5 mm. Current density−voltage (J−V) characteristics of the devices were measured using a Keithley 2420 Source Measure Unit in the dark and under AM1.5G illumination at 100 mW/cm^2 supplied by a solar simulator.

3. RESULTS AND DISCUSSION

Single-crystal FNRs were produced ultrarapidly via LLIP method at 25 °C. Methanol solution (5 mL) was slowly added into a saturated solution of C_{60} in mesitylene (1 mL; 0.99 mg/mL). A brownish-yellow color appeared immediately at the liquid interface, indicating the formation of FNRs. This method accelerates rapid large-scale production of 1D FNRs at room temperature. The overall synthetic procedure completed in just 5 s.

Figure 1a,b shows digital image of C_{60} dissolved in mesitylene and instantly formed FNRs. Figure 1c shows typical SEM images of 1D FNRs. Figure 1d,e shows histograms of length and diameter distributions of randomly selected 100 FNRs. Additional SEM images of FNRs are supplied in Figure S1, (Supporting Information). Linear rod morphology of the FNRs can be seen in Figure 1c. Histogram of length distribution shows that lengths of FNRs are in the range of 2−20 μm, and the majority of FNRs exhibit a length of ∼11 μm (Figure 1d). The histogram suggests a mean diameter of 215 nm of FNRs (Figure 1e). A high-resolution SEM image shows that the individual FNRs possess a clean surface along its entire length with clear facets (inset, Figure 1c). After the ultrarapid growth of FNRs, reaction time did not modulate the overall length and diameter of FNRs. SEM images of FNRs at different reaction times are supplied in Figures S2 (after 24 h) and S3 (after 1 week; Supporting Information). Reproducibility of FNRs is quite high. We have observed the similar structure and morphology the FNRs from five batches of synthesis.

The crystal structure of the ultrarapidly formed FNRs is confirmed by XRD analysis. The XRD patterns of as-prepared FNRs and pristine C_{60} are presented in Figure 2. The XRD

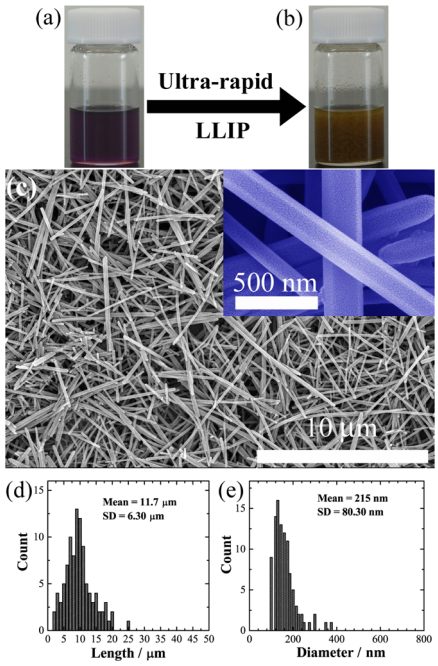

Figure 1. (a) Digital photograph of C_{60} dissolved in mesitylene, (b) digital photograph of ultrarapidly grown 1D FNRs, (c) SEM images of FNRs produced via LLIP method at an interface of methanol and saturated solution of C_{60} in mesitylene at room temperature, (c, inset) higher magnification SEM images demonstrating hexagonal faceted morphology, (d) histogram of length distribution of randomly selected 100 FNRs with mean length of 11.7 μm, and (e) histogram of FNRs diameter distribution with mean diameter of 215 nm.

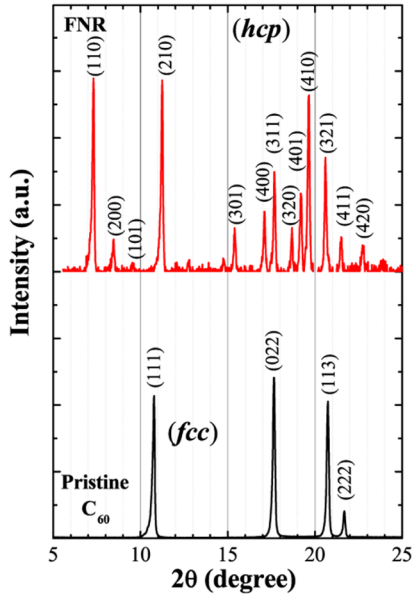

Figure 2. XRD patterns of ultrarapidly formed FNRs and pristine C_{60} powder.

patterns clearly show that the structure of ultrarapidly formed FNRs is different from face-centered cubic (*fcc*) structure of pristine C_{60} with cell dimension calculated to be a = 1.240 nm. The XRD pattern of FNRs shows reflections corresponding to (110), (200), (101), (210), (301), (400), (311), (320), (401), (410), (321), (411), and (420) planes, corresponding to the hexagonal close-pack (*hcp*) crystal structure. The cell dimensions calculated to be a = 2.401 nm and c = 1.025 nm (a/c = 2.342) are similar to the previously reported *hcp* structures of C_{60} solid solvates, demonstrating that the FNRs can be indexed to $P6_3$ space group with solvent molecules between layers with a 3-fold symmetry near the 6_3 screw axis.[36−38]

The crystal structure of FNRs is further characterized using TEM analysis. The TEM images reveal straight solid morphology of the FNRs (Figure 3a,b), which is similar to

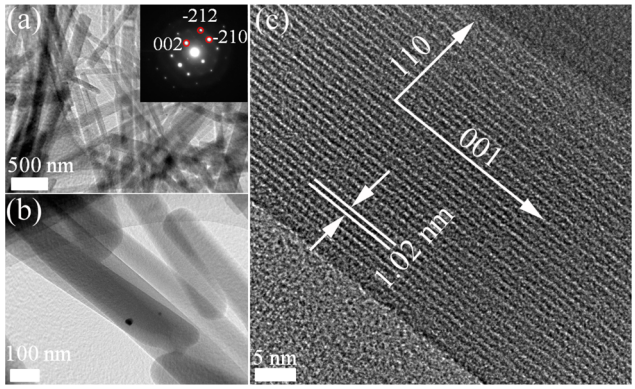

Figure 3. (a) Low-magnification TEM image displaying several FNRs solid, (a, inset) SAED pattern of a single FNR, (b) higher-magnification TEM image displaying FNR solids, (c) HR-TEM images from the thinnest area of a single FNR.

that observed in SEM analysis. Additional TEM images are supplied in Figure S4 (Supporting Information). Although there is overall variation in the diameters of FNRs, the diameter of an individual FNR remains uniform along its entire length. The selected area electron diffraction (SAED) pattern (inset, Figure 3a) and HRTEM (Figure 3c) image were taken from the thinner outer edge of a FNRs. The SAED pattern of FNRs solid shows diffraction spots suggesting a single-crystalline structure of FNRs. The diffraction spots can be indexed to (002), (−210), and (−212) crystallographic planes corresponding to the *hcp* structure. HRTEM image of the FNRs shows dense packed lattice planes parallel to the length of FNRs. The lattice spacing is ca. 1.02 ± 0.06 nm, corresponding to the distance between two (110) planes and demonstrating that the (001) axial direction is preferred growth direction of FNRs.[36,38]

Note that the observed *hcp* crystal structure of FNRs is an indication of the formation of stable 1D solid solvates with mesitylene. C_{60} solvates incorporate guest solvent molecules into the host C_{60} lattice and change the crystal structure. Many organic solvents including benzene, toluene, hexane, carbon disulfide, and xylene have been reported to form C_{60} solid solvates.[39−42] Nanostructures of C_{60} solvates represent a new type of functional materials, and they offer interesting optical, mechanical, and transport properties and are stable under pressure.[43−45] A recent report has shown that single-crystal nanowires of solvated C_{60} display electron mobility as high as 11 $cm^2\ V^{-1}\ s^{-1}$, which is ∼8 fold higher than maximum reported mobility for solution grown *n*-channel organic material, demonstrating the key importance of 1D solid solvates of C_{60} in device fabrications.[46]

The solid solvate structure of FNR crystals is further confirmed by FTIR spectroscopy. Figure 4a shows FTIR spectra of FNRs and pristine C_{60} recorded at 25 °C. In addition to four major peaks of pristine C_{60} at 527, 576, 1181, and 1429

dx.doi.org/10.1021/am5046235 | ACS Appl. Mater. Interfaces 2014, 6, 15597−15603

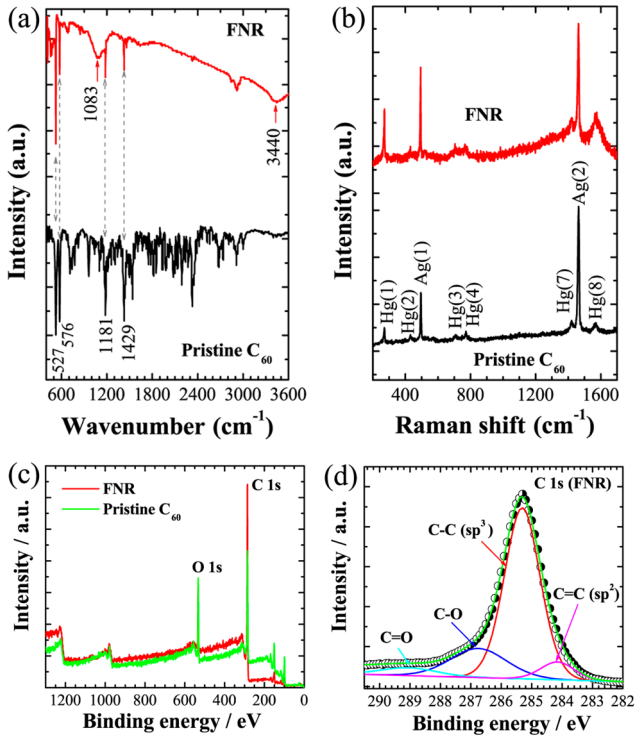

Figure 4. Comparison of (a) FTIR spectra, (b) Raman spectra, (c) XPS survey spectra of ultrarapidly produced FNRs with pristine C_{60}, and (d) C 1s deconvoluted XPS spectra of FNRs.

cm^{-1}, two additional peaks at 3440 cm^{-1} (O−H stretching) and 1083 cm^{-1} (C−O stretching vibration) can be seen in the FTIR spectrum of FNRs. This indicates that the ultrarapidly formed FNRs contain some solvent molecules, that is, they are C_{60} solvates. A thermogravimetry (TG) curve with the temperature ramped from 20 to 1050 °C at a rate of 10 °C/min in an Ar atmosphere (Figure S5, Supporting Information) clearly shows two mass loss regions in the studied range of temperatures. The first mass loss has a maximum at a temperature close to the boiling temperature of mesitylene, which shows that mass loss is due to the evaporation of solvent.

Figure 4b compares Raman scattering spectrum of pristine C_{60} and the FNRs recorded upon exciting with a 514.5 nm laser at 25 °C. Two Ag [Ag(1) and Ag(2)] and six Hg [Hg(1), Hg(2), Hg(3), Hg(4), Hg(7), and Hg(8)] vibration bands are observed in Raman spectra of both pristine C_{60} and FNRs. Note that out of all the Raman active bands, the Ag(2) band corresponding to pentagonal pinch mode, which is susceptible to intermolecular interactions, has been used extensively as an analytical probe for structural and electronic properties of C_{60} molecules. A shift of the Ag(2) band toward lower frequency is an indication of polymerization of C_{60} molecules. We noted that Ag(1), Ag(2), and Hg(1)−Hg(8) modes of C_{60} molecules remain essentially unchanged in FNRs, demonstrating that molecular C_{60} dominates in the FNRs and no polymerization takes place upon laser irradiation during measurements.[47]

Figure 4c,d shows XPS core level electronic spectra. Survey XPS spectrum of FNRs and pristine C_{60} are similar showing the presence of C and O ls core level peaks (Figure 4c). The XPS C 1s core level peak can be deconvoluted into four peaks at 284.2, 285.3, 286.7, and 289.0 eV corresponding to C═C (sp^2 carbon), C−C (sp^3), C−O, and C═O, respectively (Figure 4d). A similar C 1s core level peak is observed for pristine C_{60} demonstrating that they have common surface structure. The XPS spectrum of O 1s could also be deconvoluted into three peaks (Figure S6, Supporting Information) with peak maximum at 533.3 eV (∼94%: O−C−O), 531.6 eV (∼4%: C═O), and 534.8 eV (∼2% −OH).

The electronic structures of C_{60} in 1D FNRs and pristine C_{60} were studied using optical absorption and PL spectroscopy. Figure 5 shows the absorption spectra of pristine C_{60} and FNRs obtained from a dilute solution dispersed in isopropyl alcohol.

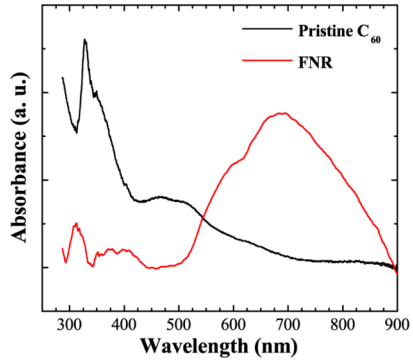

Figure 5. Absorption spectra of ultrarapidly produced FNRs and pristine C_{60}.

The absorption spectrum of C_{60} shows predominant peaks at 327 nm with a shoulder at 350 nm corresponding to allowed intramolecular electronic transitions between the HOMO and LUMO energy levels. In addition, peaks in the higher wavelengths are observed at 468, 517, and 631 nm, which might correspond to vibrational structure from one or two forbidden electronic transitions (e.g., 1Ag to 1F1g). The absorption of C_{60} is in close agreement with previous reports suggesting the exciton origin. The FNRs spectrum shows structured peaks centered at 312 and 386 nm. A broad and intense absorption feature is observed with peaks at 598 and 690 nm. The FNRs spectrum exhibits a significant increase in the absorption at longer wavelength region compared to pristine C_{60}. The distinct difference in the absorption spectra may arise from the crystalline nature and the differences in the shape of the pristine C_{60} and FNRs, which was demonstrated earlier by Jin et al.[48] These authors found that the dominance of Frenkel excitons in C_{60} evaporated films over solution phase C_{60} and C_{60} rods where charge transfer excitons play a major role in the observed optical transitions. On the contrary, we observed a dominance of Frenkel excitons in C_{60} solution over charge transfer excitons in the FNRs. Crystalline C_{60} is known to form solvated structures with the solvent owing to the presence of porous structure where the solid swells to accommodate solvent molecules resulting in a larger inter-C_{60} distance. Because the intensity of the Frenkel excitonic transitions depends on the extent of intermolecular overlap, an increase in intermolecular distance would result in the decrease of the intensity of Frenkel excitonic transitions. Hence, the solvated effect is more pronounced in the case of FNRs owing to their larger surface area compared to that of C_{60}. Additionally, the intensity of the absorption in the longer wavelength region may be attributed to the charge transfer excitonic transitions, because the intermolecular overlap increases upon increasing the conjugation length into the rods.

We have compared the PL spectra of pristine C_{60} and FNRs with the same excitation wavelength. The PL spectra of both

dx.doi.org/10.1021/am5046235 | ACS Appl. Mater. Interfaces 2014, 6, 15597−15603

pristine C_{60} and FNRs show a broad featured emission in the 600−900 nm region within which peaks appeared at 619, 682, 768, and 821 nm (Figure 6).

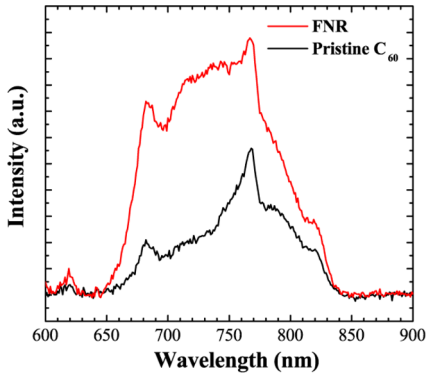

Figure 6. A comparison of PL spectra of pristine C_{60} and FNRs.

The PL peaks of C_{60} and FNRs appeared in the same positions; however, an increase in the PL intensity is observed from the FNRs. Notably, an increased absorption is also observed in the longer wavelength region leading to a substantial overlap between the emission and absorption spectra in the case of FNRs. This effect can be attributed to the Herzberg−Teller coupling between the $^3F_{1g}$ and ^1A_g states leading to increased intensity of such transitions.[48,49]

In addition to the enhancement in the PL intensity of FNRs, there is marked difference in the relative intensities of the featured PL peaks when compared with the pristine C_{60}. Additionally, a broadening of the PL is observed for the FNRs with respect to pristine C_{60}. The broadening can be attributed to the difference in the C_{60}−C_{60} interactions within the rod morphology. Because the FNRs PL spectrum contains most of the features seen in the pristine C_{60} PL spectrum, a difference in the molecular level interaction is apparent in elongated rod-shaped structures. These observations are consistent with the PL spectra of pristine C_{60} and vacuum deposited solid C_{60} film.[50−52]

Recently, considerable attention has been given to the photoresponse properties of pristine C_{60}, considering its potential use as an acceptor moiety.[53−56] The theoretical and experimental studies revealed pristine C_{60} crystals as *n*-type semiconductor. However, little is known about how the shape affects the photoconductive properties. For example, single-crystal C_{60} showed dark conductivity on the order of 10^{-8} to 10^{-6} S/m, while polycrystalline films of C_{60} show much lower conductivities owing to the grain boundaries and oxygen contamination.[57−61] To investigate the effect of shape on tailor-made C_{60} FNRs photoconductive performance, we have fabricated devices consisting of FNRs as an active layer. The FNRs layer is sandwiched between transparent anode ITO and metal cathode Al.[62] In addition, we have separately prepared devices using pristine C_{60} as an active layer in order to compare the device performances with FNRs. In both types of devices, P3HT was used as the *p*-type donor polymer and FNRs or C_{60} was used as the *n*-type acceptor. Thus, the device structures are consisting of ITO−PEDOT/PSS−P3HT−FNRs−Al or ITO−PEDOT/PSS−P3HT−C_{60}−Al. Current density versus voltage (*J*−*V*) characteristics of the devices were measured using a Keithley 2420 source measure unit in the dark and under AM1.5G illumination at 100 mW/cm^2 solar simulator.

The *J*−*V* characteristics of the devices using pristine C_{60} and FNRs under dark and light illumination are shown in Figure 7a,b. Improved device performance was observed for FNRs in

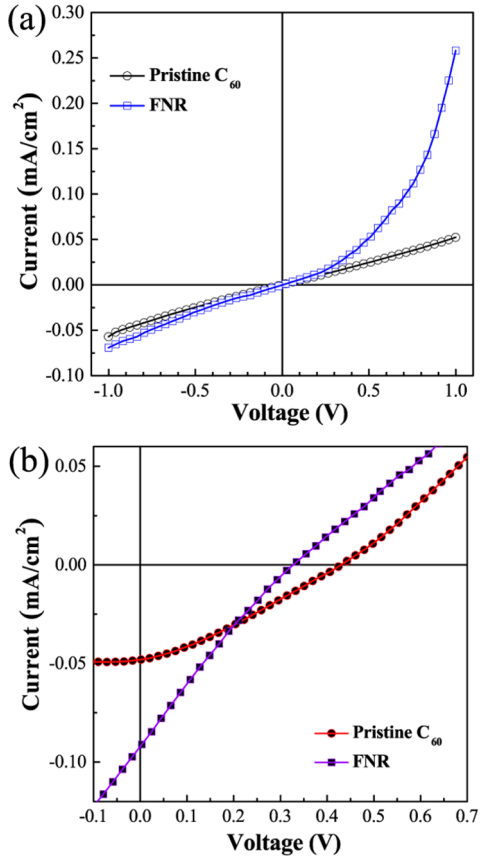

Figure 7. Comparison of (a) dark and (b) light current−voltage characteristics of pristine C_{60} and FNRs.

comparison to pristine C_{60} in the dark *J*−*V* characteristics with 6-fold enhancement of the dark current at 1 V. Upon illumination of light, both the pristine C_{60} and FNRs show photovoltaic effects showing currents in the fourth quadrant. The FNRs caused a significant enhancement of the short-circuit current (J_{SC}) from 0.05 to 0.091 mA/cm^2 in comparison to pristine C_{60}. The observed increase in J_{SC} can be interpreted counting efficient transfer of photogenerated charge carriers through stacking of C_{60} within 1D FNRs, which provides a path for charge transportation under light irradiation. Although a decrease in open-circuit voltage (V_{OC}) for FNRs devices was observed, the enhancement of the J_{SC} increases the overall fill-factor, demonstrating improved device performance in comparison to pristine C_{60}.

4. CONCLUSIONS

In summary, we have demonstrated ultrarapid formation of single-crystal C_{60} FNRs at liquid−liquid interface under ambient conditions of temperature and pressure. The entire synthetic procedure is completed in 5 s, enabling ultrarapid synthesis. The FNRs are strictly 1D with hexagonal surfaces, while the diameter along the entire length is found to be uniform. Contrary to the cubic crystal structure of pristine C_{60}, the ultrarapidly produced FNRs showed hexagonal close-pack crystal structure owing to the C_{60} solid solvate structure. The optical transitions revealed a dominance of charge transfer

excitonic transitions in 1D FNRs. An increase in the fill-factor for FNRs suggests enhanced photovoltaic properties in comparison to pristine C_{60}, revealing the effect of shape and molecular packing within the 1D structure. The large-scale, ultrarapid, room-temperature synthesis of 1D single-crystalline FNRs with excellent charge transport characteristic represents a newer type of functional materials that can be used to design tailor-made optoelectronic devices.

■ ASSOCIATED CONTENT

Supporting Information

Additional SEM and TEM images of FNRs, additional SEM images of FNRs at different reaction time, TG spectrum of FNRs, and XPS core level electronic spectrum of O 1s for FNRs. This material is available free of charge via the Internet at http://pubs.acs.org.

■ AUTHOR INFORMATION

Corresponding Authors

*E-mail: SHRESTHA.Lokkumar@nims.go.jp.
*E-mail: camsa2@iacs.res.in.

Notes

The authors declare no competing financial interest.

■ ACKNOWLEDGMENTS

L.K.S. thanks the Japan Society for the Promotion of Science (JSPS) for the Grant-in-Aid for Young Scientists B (25790021). S.A. acknowledges the financial support from the Department of Science and Technology, India.

■ REFERENCES

(1) Nakanishi, W.; Minami, K.; Shrestha, L. K.; Ji, Q.; Hill, J. P.; Ariga, K. Bioactive Nanocarbon Assemblies: Nanoarchitectonics and Applications. *Nano Today* **2014**, *9*, 378−394.
(2) Isaacson, C.; Zhang, W.; Powell, T.; Ma, X.; Bouchard, D. Temporal Changes in Aqu/C_{60} Physical-Chemical, Deposition, and Transport Characteristics in Aqueous Systems. *Environ. Sci. Technol.* **2011**, *45*, 5170−5177.
(3) Babu, S. S.; Möhwald, H.; Nakanishi, N. Recent Progress in Morphology Control of Supermolecular Fullerene Assemblies and its Applications. *Chem. Soc. Rev.* **2010**, *39*, 4021−4035.
(4) Sequra, J. L.; Martín, N.; Guldi, D. M. Materials for Organic Solar Cells: The C_{60}/π-Conjugated Oligomer Approach. *Chem. Soc. Rev.* **2005**, *34*, 31−47.
(5) Nigam, A.; Schwabegger, G.; Ulla, M.; Ahmed, R.; Fishchuk, I. I.; Kadashchuk, A.; Simbrunner, C.; Sitter, H.; Premaratne, M.; Rao, V. R. Strain Induced Anisotropic Effect on Electron Mobility in C_{60} Based Organic Field Effect Transistors. *Appl. Phys. Lett.* **2012**, *101*, 083305−4.
(6) Fischer, A.; Scholz, R.; Leo, K.; Lüssem, B. An All C_{60} Vertical Transistor for High Frequency and High Current Density Applications. *Appl. Phys. Lett.* **2012**, *101*, 213303−4.
(7) Yang, C.; Kim, J. Y.; Cho, S.; Lee, J. K.; Heeger, A. J.; Wudl, F. Functionalized Methanofullerenes Used as *n*-type Materials in Bulk-Heterojunction Polymer Solar Cells and in Field Effect Transistors. *J. Am. Chem. Soc.* **2008**, *130*, 6444−6450.
(8) Briseno, A. L.; Mannsfeld, S. C. B.; Ling, M. M.; Liu, S.; Tseng, R. J.; Reese, C.; Roberts, M. E.; Yang, Y.; Wudl, F.; Bao, Z. Patterning Organic Single-Crystal Transistor Array. *Nature* **2006**, *444*, 913−917.
(9) Kobayashi, S.-I.; Mori, S.; Iida, S.; Ando, H.; Takenobu, T.; Taguchi, Y.; Fujiwara, A.; Taninaka, A.; Shinohara, H.; Iwasa, Y. Conductivity and Field Effect Transistor of La2@C80 Metallofullerene. *J. Am. Chem. Soc.* **2003**, *125*, 8116−8117.
(10) Guérin, D.; Lenfant, S.; Godey, S.; Vuillaume, D. Synthesis and Electrical Properties of Fullerene-based Molecular Junctions on Silicon Substrate. *J. Mater. Chem.* **2010**, *20*, 2680−2690.
(11) Liu, T.; Troisi, A. What Makes Fullerene Acceptors Special as Electron Acceptors in Organic Solar Cells and How to Replace Them. *Adv. Funt. Mater.* **2013**, *25*, 1038−1041.
(12) Dong, G.; Zheng, H.; Duan, L.; Wang, L.; Qiu, Y. High-Performance Organic Optocouplers Based on a Photosensitive Interfacial C_{60}/NPB Heterojunction. *Adv. Mater.* **2009**, *21*, 2501−2504.
(13) Graham, K. R.; Cabanetos, C.; Jahnke, J. P.; Idso, M. N.; Labban, A. E.; Ndjawa, G. O. N.; Salleo, A.; Chmelka, B. F.; Amassian, A.; Beaujuge, P. M.; McGehee, M. D. Importance of the Donor:Fullerene Intermolecular Arrangement for High-Efficiency Organic Photovoltaics. *J. Am. Chem. Soc.* **2014**, *136*, 9608−9618.
(14) Mi, D.; Kim, J. H.; Kim, H. U.; Xu, F.; Hwang, D. H. Fullerene Derivatives as Electron Acceptors for Organic Photovoltaic Cells. *J. Nanosci. Nanotechnol.* **2014**, *14*, 1064−1084.
(15) Guldi, D. M. Fullerenes: Three Dimensional Electron Acceptor Materials. *Chem. Commun.* **2000**, 321−327.
(16) Brown, P.; Kamat, P. V. Quantum Dot Solar Cells. Electrophoretic Deposition of CdSe−C_{60} Composite Films and Capture of Photogenerated Electrons with nC_{60} Cluster Shell. *J. Am. Chem. Soc.* **2008**, *130*, 8890−8891.
(17) Xing, Y. J.; Jing, G. Y.; Xu, J.; Yu, D. P.; Liu, H. B.; Li, Y. L. Electrical Conductivity of a Single C_{60} Nanotube. *Appl. Phys. Lett.* **2005**, *87*, 263117−3.
(18) Vavro, J.; Llaguno, M. C.; Satishkumar, B. C.; Luzzi, D. E.; Fischer, J. E. Electrical and Thermal Properties of C_{60}-Filled Single-Wall Carbon Nanotubes. *Appl. Phys. Lett.* **2002**, *80*, 1450−3.
(19) Saran, R.; Stolojan, V.; Curry, R. J. Ultrahigh Performance C_{60} Nanorod Large Area Flexible Photoconductor Devices via Ultralow Organic and Inorganic Photodoping. *Sci. Rep.* **2014**, *4*, 5041−9.
(20) Shin, H. S.; Yoon, S. M.; Tang, Q.; Chon, B.; Joo, T.; Choi, H. C. Highly Selective Synthesis of C_{60} Disks on Graphite Substrate by a Vapor−Solid Process. *Angew. Chem., Int. Ed.* **2008**, *47*, 693−696.
(21) Geng, J.; Zhou, W.; Skelton, P.; Yue, W.; Kinloch, I. A.; Windle, A. H.; Johnson, B. F. G. Crystal Structure and Growth Mechanism of Unusually Long Fullerene (C_{60}) Nanowires. *J. Am. Chem. Soc.* **2008**, *130*, 2527−2534.
(22) Wang, L.; Liu, B.; Liu, D.; Yao, M.; Hou, Y.; Yu, S.; Cui, T.; Li, D.; Zou, G.; Iwasiewicz, A.; Sundqvist, B. Synthesis of Thin, Rectangular C_{60} Nanorods Using *m*-Xylene as a Shape Controller. *Adv. Mater.* **2006**, *18*, 1883−1888.
(23) Tachibana, M.; Kobayashi, K.; Uchida, T.; Kojima, K.; Tanimura, M.; Miyazawa, K. Photo-Assisted Growth and Polymerization of C_{60} Nanowhiskers. *Chem. Phys. Lett.* **2003**, *374*, 279−285.
(24) Liu, H.; Li, Y.; Jiang, L.; Luo, H.; Xiao, S.; Fang, H.; Li, H.; Zhu, D.; Yu, D.; Xu, J.; Xiang, B. Imaging As-Grown [60]Fullerene Nanotubes by Template Technique. *J. Am. Chem. Soc.* **2002**, *124*, 13370−13371.
(25) Masuhara, A.; Tan, Z.; Kasai, H.; Nakanishi, H.; Oikawa, H. Fullerene Fine Crystals with Unique Shapes and Controlled Size. *Jpn. J. Appl. Phys.* **2009**, *48*, 050206−3.
(26) Park, C.; Song, H. J.; Choi, H. C. The Critical Effect of Solvent Geometry on the Determinatoin of Fullerene (C_{60}) Self-Assembly into Dot, Wire, and Disk Structures. *Chem. Commun.* **2009**, 4803−4805.
(27) Shrestha, L. K.; Ji, Q.; Mori, T.; Miyazawa, K.; Yamauchi, Y.; Hill, J. P.; Ariga, K. Fullerene Nanoarchitectonics: From Zero to Higher Dimensions. *Chem.—Asian J.* **2013**, *8*, 1662−1679.
(28) Miyazawa, K.; Kuwasaki, Y.; Obayashi, A.; Kuwabara, M. C_{60} Nanowhiskers Formed by the Liquid-Liquid Interfacial Precipitation Method. *J. Mater. Res.* **2002**, *17*, 83−88.
(29) Miyazawa, K.; Hamamoto, K.; Nagata, S.; Suga, T. Structural Investigation of the C_{60}/C_{70} Whiskers Fabricated by Forming Liquid−Liquid Interfaces of Toluene with Dissolved C_{60}/C_{70} and Isopropyl Alcohol. *J. Mater. Res.* **2003**, *18*, 1096−1103.

(30) Sathish, M.; Miyazawa, K.; Sasaki, T. Nanoporous Fullerene Nanowhiskers. *Chem. Mater.* **2007**, *19*, 2398−2400.
(31) Jeong, J.; Kim, W. S.; Park, S. I.; Yoon, T. S.; Chung, B. H. Synthesis and Characterization of Various-Shaped C_{60} Microcrystals Using Alcohols as Antisolvents. *J. Phys. Chem. C* **2010**, *114*, 12976−12981.
(32) Sathish, M.; Miyazawa, K.; Hill, J. P.; Ariga, K. Solvent Engineering for Shape-Shifter Pure Fullerene (C_{60}). *J. Am. Chem. Soc.* **2009**, *131*, 6372−6373.
(33) Shrestha, L. K.; Hill, J. P.; Tsuruoka, T.; Miyazawa, K.; Ariga, K. Surfactant-Assisted Assembly of Fullerene (C_{60}) Nanorods and Nanotubes Formed at a Liquid−Liquid Interface. *Langmuir* **2013**, *29*, 7195−7202.
(34) Shrestha, L. K.; Sathish, M.; Hill, J. P.; Miyazawa, K.; Tsuruoka, T.; Sanchez-Ballester, N.; Honma, I.; Ji, Q.; Ariga, K. Alcohol-Induced Decomposition of Olmstead's Crystalline Ag(I)-Fullerene Heteronanostructure Yield Bucky Cubes. *J. Mater. Chem. C* **2013**, *1*, 1174−1181.
(35) Shrestha, L. K.; Yamauchi, Y.; Hill, J. P.; Miyazawa, K.; Ariga, K. Fullerene Crystals with Bimodal Pore Architectures Consisting of Macropores and Mesopores. *J. Am. Chem. Soc.* **2013**, *135*, 586−589.
(36) Ramm, M.; Luger, P.; Zobel, D.; Duczek, W.; Boeyens, J. C. A. Static Disorder in Hexagonal Crystal Structure of C_{60} at 100 K and 20 K. *Cryst. Res. Technol.* **1996**, *31*, 43−53.
(37) Minato, J.; Miyazawa, K. Solvated Structures of C_{60} Nanowhiskers. *Carbon* **2005**, *43*, 2837−2841.
(38) Rana, M.; Bharathanatha, R. R.; Gautam, U. K. Kinetically Stabilized C_{60}−Toluene Solvate Nanostructures with a Discrete Absorption Edge Enabling Supramolecular Topotactic Molecular Exchange. *Carbon* **2014**, *74*, 44−53.
(39) He, H.; Barras, J.; Foulkes, J.; Klinowski, J. Solid-State NIMS Studies of Fullerene C_{60}/Benzene Solvates. *J. Phys. Chem. B* **1997**, *101*, 117−122.
(40) Toscani, S.; Allouchi, H.; Tamarit, J. L.; López, D. O.; Barrio, M.; Agafonov, V.; Agafonov, V.; Rassat, A.; Szwarc, H.; Céolin, R. Decagonal C_{60} Crystals Grown from *n*-Hexane Solutions: Solid-State and Aging Studies. *Chem. Phys. Lett.* **2000**, *330*, 491−496.
(41) Tan, Z.; Masuhara, A.; Kasai, H.; Nakanishi, H.; Oikawa, H. Thermal-Induced Shape Transformation of Solvated C_{60} Microcrystals. *Carbon* **2013**, *64*, 370−376.
(42) Larsen, C.; Barzegar, H. R.; Nitze, F.; Wagberg, T.; Edman, L. On the Fabrication of Crystalline C_{60} Nanorod Transistors from Solution. *Nanotechnology* **2012**, *23*, 344015−344024.
(43) Wang, L.; Liu, B.; Li, H.; Yang, W.; Ding, Y.; Sinogeikin, S. V.; Meng, Y.; Liu, Z.; Zeng, X. C.; Mao, W. L. Long-Range Ordered Carbon Clusters: A Crystalline Material with Amorphous Building Blocks. *Science* **2012**, *337*, 825−828.
(44) Wang, L.; Liu, B.; Yu, S.; Yao, M.; Liu, D.; Hou, Y.; Cui, T.; Zou, G.; Sundqvist, B.; You, H.; Zhang, D.; Ma, D. Highly Enhanced Luminescence from Single-Crystalline C_{60}·1*m*-Xylene Nanorods. *Chem. Mater.* **2006**, *18*, 4190−4194.
(45) Asaka, K.; Kato, R.; Miyazawa, K.; Kizuka, T. Buckling of C_{60} Whiskers. *Appl. Phys. Lett.* **2006**, *89*, 071912−3.
(46) Li, H. Y.; Tee, B. C. K.; Cha, J. J.; Cui, Y.; Chung, J. W.; Lee, S. Y.; Bao, Z. N. High-Mobility Field-Effect Transistors from Large-Area Solution-Grown Aligned C_{60} Single Crystals. *J. Am. Chem. Soc.* **2012**, *134*, 2760−2765.
(47) Kuzmany, H.; Matus, M.; Burger, B.; Winter, J. Raman Scattering in C_{60} Fullerenes and Fullerides. *Adv. Mater.* **1994**, *6*, 731−745.
(48) Jin, Y.; Curry, R. J.; Sloan, J.; Hatton, R. A.; Chong, L. C.; Blanchard, N.; Stolojan, V.; Kroto, H. W.; Silva, S. R. P. Structural and Optoelectronic Properties of C_{60} Rods Obtained via a Rapid Synthesis Route. *J. Mater. Chem.* **2006**, *16*, 3715−3720.
(49) Wang, Y.; Holden, J. M.; Rao, A. M.; Eklund, P. C.; Venkateswaran, U. D.; Eastwood, D.; Lidberg, R. L.; Dresselhaus, G.; Dresselhaus, M. S. Optical Absorption and Photoluminescence in Pristine and Photopolymarized C_{60} Solid Films. *Phys. Rev. B: Condens. Matter Mater. Phys.* **1995**, *51*, 4547−4556.
(50) Capozzi, V.; Trovato, T.; Berger, H.; Lorusso, G. F. Photoluminescence Spectra of C_{60} Thin Films Deposited on Different Substrates. *Carbon* **1997**, *35*, 763−766.
(51) Sun, Y. P.; Wang, P.; Hamilton, N. B. Fluorescence Spectra and Quantum Yields of Buckminsterfullerene (C_{60}) in Room-Temperature Solutions. No Excitation Wavelength Dependence. *J. Am. Chem. Soc.* **1993**, *115*, 6378−6381.
(52) Wang, Y. Photophysical Properties of Fullerene and Fullerene/*N*,*N*-Diethylaniline Charge-Transfer Complexes. *J. Phys. Chem.* **1992**, *96*, 764−767.
(53) Yi, Y.; Coropceanu, V.; Brédas, J.-L. Exciton-Dissociation and Charge-Recombination Processes in Pentacene/C_{60} Solar Cells: Theoretical Insight into the Impact of Interface Geometry. *J. Am. Chem. Soc.* **2009**, *131*, 15777−15783.
(54) Chan, S.-H.; Lai, C.-S.; Chen, H.-L.; Ting, C.; Chen, C.-P. Highly Efficient P3HT: C_{60} Solar Cell Free of Annealing Process. *Macromolecules* **2011**, *44*, 8886−8891.
(55) Ratcliff, E. L.; Zacher, B.; Armstrong, N. R. Selective Interlayers and Contacts in Organic Photovoltaic Cells. *J. Phys. Chem. Lett.* **2011**, *2*, 1337−1350.
(56) Graham, K. R.; Cabanetos, C.; Jahnke, J. P.; Idso, M. N.; Labban, A. E.; Ndjawa, G. O. N.; Heumueller, T.; Vandewal, K.; Salleo, A.; Chmelka, B. F.; Amassian, A.; Beaujuge, P. M.; McGehee, M. D. Importance of the Donor:Fullerene Intermolecular Arrangement for High-Efficiency Organic Photovoltaics. *J. Am. Chem. Soc.* **2014**, *136*, 9608−9618.
(57) Wen, C.; Li, J.; Kitazawa, K.; Aida, T.; Honma, I.; Komiyama, H.; Yamada, K. Electrical Conductivity of a Pure C_{60} Single Crystal. *Appl. Phys. Lett.* **1992**, *61*, 2162−2163.
(58) Yang, C. M.; Liao, J. L.; Chiu, K. C. Diffusion of O_2 in C_{60} Crystal by Measuring the Decay of Electrical Conductivity. *J. Appl. Phys.* **2004**, *96*, 1934−1938.
(59) Gong, J. L.; Zhang, F. Q.; Li, Y. H.; Ma, G. B.; Chen, G. H. Effect of Annealing on the Electrical Conductivity of C_{60} Films. *Thin Solid Films* **1995**, *261*, 266−270.
(60) Hamed, A.; Sun, Y. Y.; Tao, Y. K.; Meng, R. L.; Hor, P. H. Effects of Oxygen and Illumination on the in Situ Conductivity of C_{60} Thin Films. *Phys. Rev. B: Condens. Matter Mater. Phys.* **1993**, *47*, 10873−10880.
(61) Mort, J.; Machonkin, M.; Ziolo, R.; Huffman, D. R.; Ferguson, M. I. Temperature Dependence of Photoconductivity in Buckminsterfullerene Films. *Appl. Phys. Lett.* **1992**, *60*, 1735−1737.
(62) Wang, X.; Liow, C.; Qi, D.; Zhu, B.; Leow, W. R.; Wang, H.; Xue, C.; Chen, X.; Li, S. Programmable Photo-Electrochemical Hydrogen Evolution Based on Multi-Segmented CdS-Au Nanorod Arrays. *Adv. Mater.* **2014**, *26*, 3506−3512.